Journal of Power Sources 590 (2024) 233802

Contents lists available at ScienceDirect

Journal of Power Sources

journal homepage: www.elsevier.com/locate/jpowsour

# Effects of mechanical pressure on anion exchange membrane water electrolysis: A non-negligible yet neglected factor

Lu Xia [a,1], Sebastian Holtwerth [a,b], Christian Rodenbücher [a], Werner Lehnert [a,b], Meital Shviro [a,2], Martin Müller [a,*]

[a] Institute of Energy and Climate Research, Electrochemical Process Engineering (IEK-14), Forschungszentrum Jülich GmbH, 52425, Jülich, Germany
[b] Faculty of Mechanical Engineering, RWTH Aachen University, 52062, Aachen, Germany

## HIGHLIGHTS

- Dependence of cell mechanics, mass transport, wettability over contact pressure.
- Electrochemical performance and internal resistance in the pressure range 0–6 MPa.
- 0.5 MPa is optimal contact pressure to suppress $R_{\Omega}/R_{ct}$ and relieve $R_{md}$.
- Membrane thickness (≥50 μm) favorable to prevent membrane damage.
- Pre-assembly and gradually increased mechanical pressure are esential for mounting.

## GRAPHICAL ABSTRACT

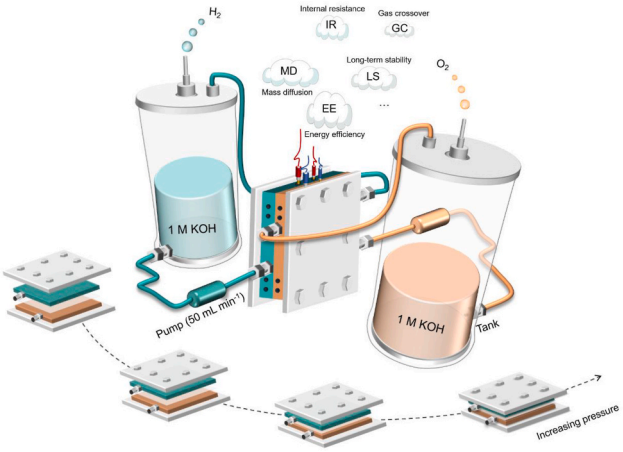


## ARTICLE INFO

*Keywords:*
Mechanical pressure
Porous electrodes
Anion exchange membrane water electrolysis

## ABSTRACT

Commercialized implementations of anion exchange membrane water electrolysis (AEMWE) require stable operation at high current density. To achieve this, ohmic, electrochemical and concentration polarizations are supposed to be exceedingly suppressed. Among all crucial materials, porous electrodes with catalyst coatings extensively affect the above polarizations, which are highly sensitive to specific mechanical pressure for cell assembly. However, the imposed mechanical pressure and its effects on cell performance are rarely reported in AEMWE cells. Here, quantitative characterizations of mechanical pressure and its effects on ***i)*** physical properties of catalyst coated electrodes and ***ii)*** corresponding single-cell performance are comprehensively investigated. First, the imposed mechanical pressure on membrane electrode assembly (MEA) is controlled by different total thickness gaps between anode/cathode and poly-tetra-fluoroethylene (PTFE) gaskets (Δd = 0, 100, 200, 300

* Corresponding author.
*E-mail address:* mar.mueller@fz-juelich.de (M. Müller).
[1] Present Address: ICFO–Institut de Ciències Fotòniques, The Barcelona Institute of Science and Technology, 08860 Castelldefels, Barcelona, Spain.
[2] Present Address: Chemistry and Nanoscience Center, National Renewable Energy Laboratory (NREL), Golden, CO, 80401, United States.

https://doi.org/10.1016/j.jpowsour.2023.233802
Received 3 July 2023; Received in revised form 26 October 2023; Accepted 29 October 2023
Available online 9 November 2023

μm). Second, the above resulted distributions of mechanical pressure are quantitatively studied by a mechanical pressure tracking method. Third, the influence of the mechanical pressure on the physical properties of the electrodes and cell performance are demonstrated. It is proved that the mechanical pressure of ca. 0.5 MPa is comprehensively beneficial for suppressing internal resistance ($R_\Omega$) and charge transfer resistance ($R_{ct}$), with slightly increased mass diffusion resistance ($R_{md}$) and hydrogen crossover. This study unveils the intrinsic effects of mechanical pressure on cell performance and provides critical insights into baseline benchmarking and single-cell even stack optimization.

## 1. Introduction

Water electrolysis powered by renewable energy for hydrogen ($H_2$) generation offers promising solutions to environmental pollution, climate change, and energy crisis [1–4]. Classic alkaline water electrolysis (CAWE) as a grid-scale technology is fully commercialized, owing to its superior stability and low-cost key materials, like diaphragm, nickel-based catalysts *etc.*, which, however, can only be operated at a low current density of 200–400 mA $cm^{-2}$ for a decent energy efficiency [5,6]. To break this limitation, proton exchange membrane water electrolysis (PEMWE) [7], anion exchange membrane water electrolysis (AEMWE) [8], and bipolar-membrane water electrolysis (BPMWE) [9] have been considered as attractive candidates. Among them, PEMWE is the most mature technology but highly hindered by the scarcity and high cost of platinum group metal (PGM)-based catalysts for further market penetration [10], while BPMWE is still in the early concept stage with the main challenge of specific membrane stability [11]. In addition, AEMWE attracts increasing interests due to the utilization of low-cost, PGM-free catalysts, thus higher scalability than PEMWE. Meanwhile, with highly conductive AEM in moderate electrolytes of 0–1.0 M KOH, AEMWE shows higher operating current than CAWE (Fig. S1).

Compared with PEMWE, the main technical barriers of AEMWE lie in its limited technology readiness level (TRL) *etc.* [12–16] The optimization of testing conditions, membrane electrode assembly (MEA) has played a pivotal role in advancing TRL for its commercilization. Testing conditions exhibit a tremendous impact on activity and stability. Niaz et al. studied the impact of operating time for AEMWE and concluded better stability can be achieved in longer-term operation [17]. Howerver, they have not yet optimized the impact of mechanical pressure. In fact, the mechanical pressure for cell assembly was hardly mentioned in AEMWE and quite a few papers referred to mechanical pressure, without the understanding of its effects on electrodes and cell performance. Xu et al. pioneered on studying the anodic and cathodic potentials by adding reference electrode in the full cell, finding that the potential of both electrodes changed simultaneously if the gasket on the cathode side was removed. This means gasket is crucially important to internal mechanical pressure, thus affecting the anode performance [18]. However, they did not investigate the effects of mechanical pressure on electrodes and cell performance such as stability and hydrogen crossover, *etc.* Unquantified mechanical pressure caused a big difference in the benchmark of cell performance among groups even with standard commercial materials [19–21]. Encouraged by the strong effects of mechanical pressure on the internal resistance ($R_\Omega$), mass diffusion ($R_{md}$) resistance and charge transfer resistance ($R_{ct}$) in PEMWE or redox flow batteries [22], we propose to study the distribution of mechanical pressure and its comprehensive effects on cell performance of AEMWE.

In this study, a tracking method is utilized to quantify the applied mechanical pressure on the cell to describe its distribution. The thickness of PTFE is found to be a decisive factor to the mechanical pressure and the external torque interact with different thickness of PTFE is finally transformed to pressure distribution. Moreover, the cell performance based on two different membranes is extensively investigated to understand the effects of mechanical pressure on contact, charge transfer and mass transfer resistance, and gas permeation, *etc.* The activity of the cell is fully maximized with ensured safety (<2 vol% $H_2$ in $O_2$) and stability (Fig. 1). Finally, overall better mechanical pressure for cell assembly is highly recommended to boost the comprehensive cell performance. This study also provides a reference to benchmark and optimize cell or even stack assembly for AEMWE.

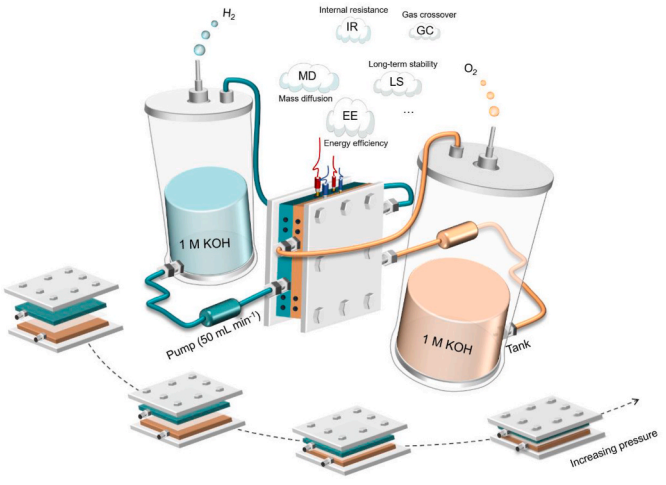


**Fig. 1.** The cell configuration and the mechanical pressure dependent performances in 1 M KOH with the flowing rate of 50 mL $min^{-1}$, such as contact or internal resistance, mass diffusion in gas diffusion layer, stability during long-term operation, and corresponding gas crossover *etc.*

## 2. Materials and methods

### 2.1. Materials

Carbon paper and nickel-based gas diffusion layers (GDL, thickness: 500 μm; porosity: 66%; pore size: 32 μm and fiber diameter: 22 μm) were supplied from Toray Industries Inc. (Japan) and NV Bekaert SA (Belgium). Anion exchange membranes (Aemion+™, AF1-HNN5-25, AF1-HNN8-50) and ionomer (AP1-HNN8-00-X) were supplied from Ionomr Innovations Inc (Canada). Platinum (Pt/C, 60% Pt) and iridium black (Ir, 99.99%) were used as received from Alfa Aesar, and Fuel Cell Store. Potassium hydroxide (KOH, ≥85.0%, EMSURE®) was purchased from Merck KGaA (Germany).

### 2.2. Electrode preparation

Cathodes and anodes were nickel fiber/iridium (2.2*2.3 = 5.0 $cm^2$, 1 mg $cm^{-2}$) and carbon paper/Pt/C (2.2*2.3 = 5.0 $cm^2$, 0.8 mg $cm^{-2}$) fabricated by spray coater (Sono-Tek, USA) with the spraying rate of 0.3 mL $min^{-1}$ at the temperature of 80 °C. The ink for cathodes was composed of Pt/C (75 wt%) and ionomer (25%) dispersed in the solvent D.I. water and ethanol with the mass ratio of 1:1, while that for anodes was iridium (80%) and ionomer (20%) in the same solvent.

### 2.3. Mechanical pressure measurements

Mechanical pressure measurements were achieved by color imprint of three different mechanical pressure-sensitive foils in the cells

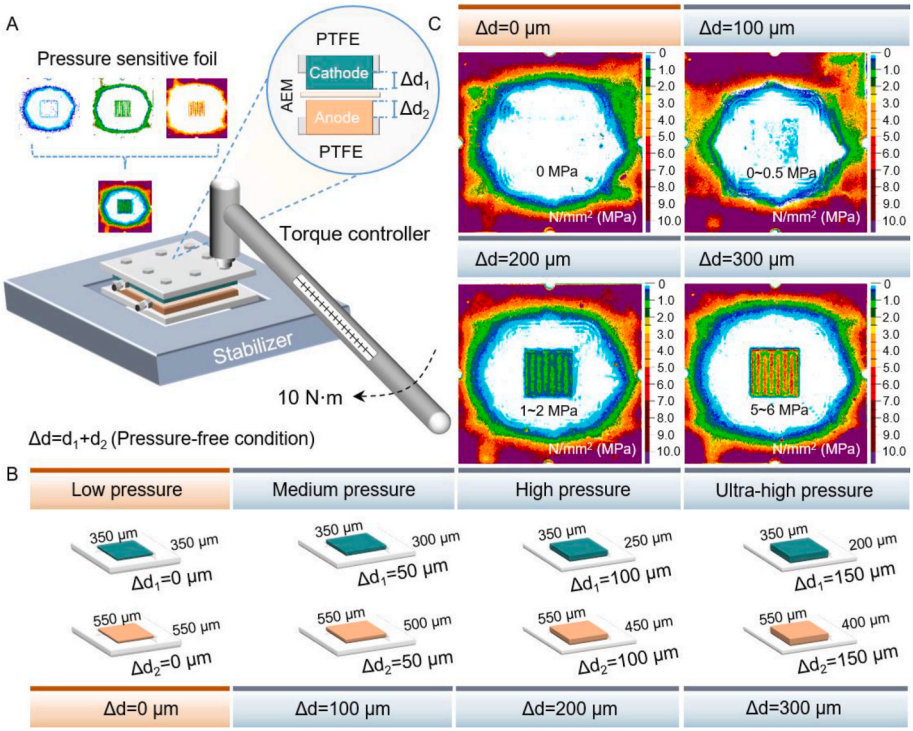


**Fig. 2.** (A) Schematic illustration of the cell assembly on a stabilizer by a torque controller with the value of 10 N m. The initial thickness of anode and cathode is 550 and 350 μm with different thickness of PTFE as gaskets and the gap is marked as $\Delta d = \Delta d_1 + \Delta d_2$ ($\Delta d_1$ and $\Delta d_2$ denote the variations before cell assembly in electrode and PTFE sealing thickness of the cathode and anode correspondingly. The cumulative thickness, Δd, results from the summation of $\Delta d_1$ and $\Delta d_2$). (B) The relationship between the distribution of mechanical pressure from low, medium, high to ultra-high pressure and Δd from 0, 100, 200–300 μm. (C) The resulted mechanical pressure distribution after cell assembly with different thickness of PTFE.

assembled by different Δd from 0, 100, 200, to 300 μm, and the final distributions of mechanical pressure were obtained through scanning, statistical analysis.

### 2.4. Physical properties

#### 2.4.1. Thickness, bulk + contact resistance, contact angle

The electrodes after different mechanical pressure treatments (Δd = 0, 100, 200, and 300 μm) were prepared by assembling and opening the cells. The thickness of all electrodes was tested by the tester for 5 times at different sites and averaged with error bars. Bulk + contact resistance was tested by Ohm's Law in a simple circuit, consisting of two copper (Cu) sheets and one electrode at the current of 15 A, and then calibrated by the resistance of Cu and circuit.

#### 2.4.2. Morphologies

Three-dimensional 4 K microscope (VHX-7000, KEYENCE) was applied to study the roughness and thickness distribution of electrodes. Optical microscope was initially used to detect changes in electrodes before and after compression. More detailed morphologies were further captured by field emission scanning electron microscope (LEO 1550 VP, ultra-high-resolution VP FE-SEM).

### 2.5. Single-cell tests

#### 2.5.1. Configuration of cell-testing system

The electrolysis system consists of auxiliary facilities including pumps, electrolyte tanks, heating, water compensation, gas handling devices and single cells that consist of sandwich-structured Pt/C//AEM//Ir, PTFE, bipolar plates and end plates. Cell assembly was achieved by a torque controller according to the principle of diagonal and step-by-step compression. KOH was dissolved in D.I. water as electrolyte with the concentration of 1 M (1044.8979 kg/m$^3$ at 25 °C) confirmed by density test instrument (DMA™ 35, Anton Paar Inc.) The electrolyte pumping rate was 50 mL min$^{-1}$ (10 mL min$^{-1}$ cm$^{-2}$). Cell temperature was stabilized at 60 ± 1 °C.

#### 2.5.2. Testing steps

Firstly, all cells went through the same conditioning steps: 1. open circuit voltage (2 h); constant voltage at 1.7 V (6 h). Secondly, polarization curves were conducted by a galvanostatic method (5 min step$^{-1}$), and the stabilized voltage at each stage was picked out for an equilibrium polarization curve. Three repetitions and corresponding error bars were required. Then, short-term stability was tested at a constant current density of 1000 mA cm$^{-2}$, during which the gas crossover (GC) was also monitored by a GC system (490, Agilent Technologies). After that, galvanostatic intermittent titration technique (GITT) curves were tested by applying alternating electrolysis (1000 mA cm$^{-2}$ for 5 min) and relaxation (open circuit voltage (OCV) for 0.5 min).

#### 2.5.3. Study of mechanical pressure

The effects of mechanical pressure were studied by using two parallel cells (Fig. S2A) with the same structure sealed by eight screws in a square distribution and two serpentine channels for electrolyte flow (Fig. S2B). The main parts of the cell for assembly are shown in Fig. S2C, and the method of spray coating at 80 °C was used for catalyst coated substrates (CCSs). The pathways for sprayer were horizontally and vertically alternative serpentines (Figs. S3A–C). The resulted CCSs showed the thickness of 350 μm for the cathode, while 550 μm for the anode (Figs. S3D and E). As for assembly, the end plate of the cell was fixed on a plastic stabilizer, and the pressure was applied by a torque controller (Fig. 2A). PTFE gaskets with four types of thickness from 250 to 350 μm with the increment of 50 μm were utilized for cell sealing. The thickness gaps between PTFE and electrode before cell assembly were $\Delta d_1$ for the cathode and $\Delta d_2$ for the anode, while the whole thickness gap from both sides was denoted as $\Delta d = d_1 + d_2$ with the value of 0, 100,

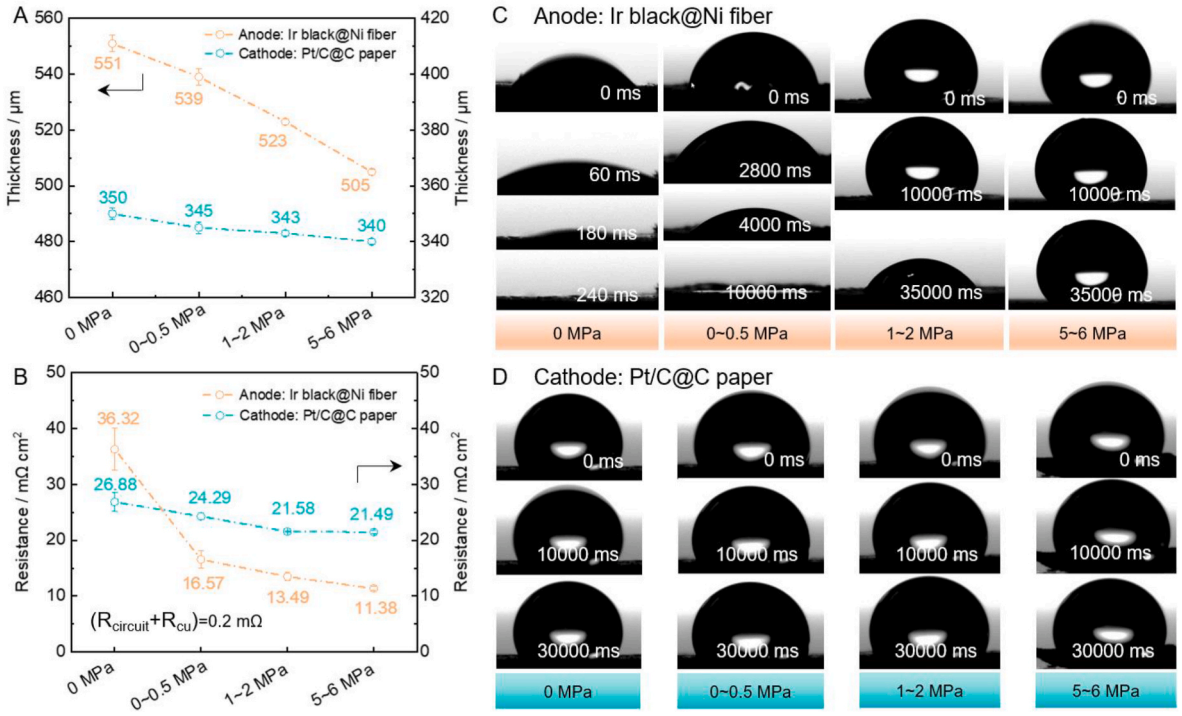


**Fig. 3.** The physical properties of the electrodes after cell assembly with different mechanical pressure from 0, 0~0.5, 1–2 to 5–6 MPa. The cell after mechanical pressure treatment was open and the electrode was taken out for characterizations: (A) Thickness, (B) integrated value of bulk and contact resistance of anodes and cathodes, and (C) corresponding contact angles.

200 and 300 μm. To reduce the contributing factors, $\Delta d_1$ and $\Delta d_2$ were equal to each other. The definition of Δd only refers to the total gaps before cell assembly and was tested without compression, which facilitates to repeat the cell assembly process despite decreased Δd after cell compression.

The cell assembly for the measurement of mechanical pressure according to the above Δd from 0–300 μm. Then, mechanical pressure was recorded by three sensitive foils with different pressure sensitivity. Finally, pressure distribution was presented after scanning and integrating. The cells under different mechanical pressure conditions are designed to low (Δd = 0 μm), medium (Δd = 100 μm), high (Δd = 200 μm), and ultra-high pressure (Δd = 300 μm) (Fig. 2B).

## 3. Results and discussions

The tracked mechanical pressure are shown in Fig. 2C with color mapping in three pressure ranges. The areas around screws are concentrated with purple imprint, indicating the highest mechanical pressure ≥10 MPa. Meanwhile, the areas around MEA-PTFE borders show white imprint, indicating it is a pressure-free zone due to electrode-PTFE gaps. The mechanical pressure on the middle of MEA zone is not evenly distributed due to that porous electrodes invade into electrolyte channels. The mechanical pressure on the solid part of the flow field is much higher than that on the hollow part. To simplify, the mechanical pressure reflected on the solid part is calculated as the pressure on MEA. In Fig. 2C, it is clear that Δd is a determining factor to mechanical pressure distribution, and the corresponding pressure ranges are as follows: 0 MPa with Δd = 0 μm, 0~0.5 MPa with Δd = 100 μm, 1.0–2.0 MPa with Δd = 200 μm, 5.0–6.0 MPa with Δd = 300 μm. To be specific, the cell with Δd = 0 μm shows negligible pressure imprint caused by less space for compression and the incompressibility of PTFE. On this condition, inadequate contact between the electrode and current collector may cause high contact resistance [23], while long-range migration of ions also has impact on charge transfer resistance [24], which has to be further demonstrated in polarization performance of electrolyzers. With Δd increasing to 100 μm, the mechanical pressure increases to ca. 0~0.5 MPa with uniform distribution, which can be caused by the surface roughness that will be proved by physical characterizations of electrodes. To alleviate, preloading, unloading and then reloading the torque for can be followed to achieve better mechanical pressure distribution. With Δd increasing to 200 and 300 μm, the mechanical pressure further increases, but not follow a linear trend, especially with Δd from 200 μm (1.0–2.0 MPa) to 300 μm (5.0–6.0 MPa). When Δd is equal to or higher than 200 μm, the mechanical pressure imprint on hollow channel areas turning to green (ca. 1.0 MPa), indicating electrode invasion happens. Severe electrode intrusion means less space for ion and gas diffusion, thus blocking mass transfer processes especially during long-term, high-current electrolysis, which will be further discussed in stability of electrolyzers [25].

Mechanical pressure has remarkable impacts on the physical properties of both anode and cathode. First, the thickness of cathode decreases by 2.86% while 8.35% for the anode with the mechanical pressure from 0 to 5–6 MPa, indicating anodic nickel fiber is more sensitive to mechanical pressure than cathodic carbon paper (Fig. 3A), while it is also possibly due to that the whole thickness of cathode is 200 μm lower than that of the anode. The error of thickness decreases with higher mechanical pressure, which can be explained by progressively decreased surface roughness. Then the contact resistance including the bulk resistance, denoted as $R_{b+c}$, was tested in a home-made configuration with the anode in the middle of two cupper plates under high current of 15 A (Fig. S4) [25]. Since mechanical pressure also has an impact on the bulk resistance of the electrode, it was, for convenience, considered as a whole with the contact resistance. Similarly, it is also more sensitive for the anodic $R_{b+c}$ than that of the cathode to mechanical pressure, with a much higher decrease rate by 68.3% and 20.1% with the mechanical pressure from 0 to 5–6 MPa, (Fig. 3B). More specific, the anodic $R_{b+c}$ decreases first by 54.4% from 0 to 0~0.5 MPa, while the cathodic counterpart drops only 9.6%, indicating contributing effects of substrate materials to mechanical pressure. Other than substrate materials, the anodic wetting performance is also more sensitive

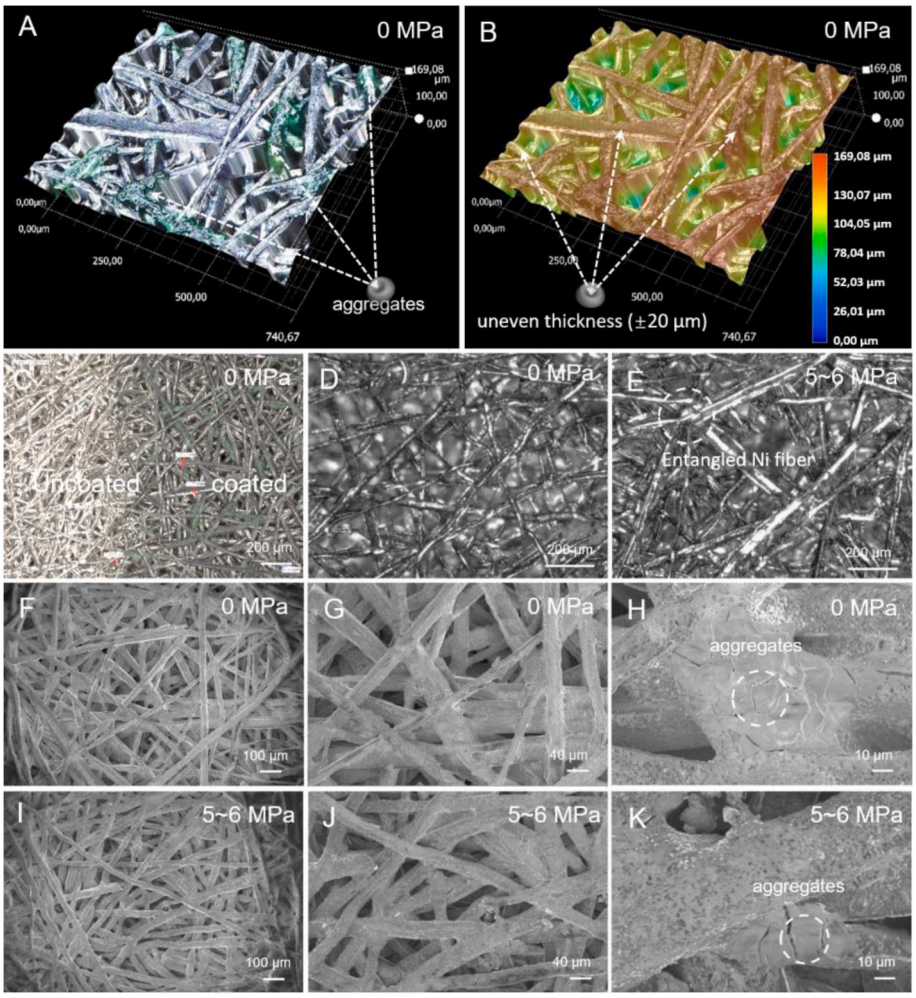


**Fig. 4.** The images of iridium black coated electrode prepared by the pressure of 0 MPa, captured by a digital microscope: (A) three-dimension (3D) microstructure of ionomer and iridium on nickel fibers. (B) The distribution of surface roughness, and (C) two-dimension (2D) morphologies before and after spray coating. The images of electrodes before and after compression captured by an optical microscope: (D–E) anodes prepared under mechanical pressure of 0 and 5–6 MPa. SEM images of anodes prepared under mechanical pressure of 0 (F–H) and 5–6 MPa (I–K) with views at three magnifications.

than cathodic counterpart to mechanical pressure, demonstrated by water contact angles (Fig. 3C and D). The anodic and cathodic water contact angles are 30 ± 10° and 130 ± 5°, indicating more hydrophilic surface of the anode [26]. The wetting time of the anode shorts sharply from 240 ms for full wetting (0 MPa) to 35000 ms for unwetting (5–6 MPa). Meanwhile, the wetting time of cathode shows negligible difference before and after compression. These indicate the anodic surface microstructure change much faster than cathodic counterpart. Considering the above differential results, we focus more on anodic properties in the following parts.

The 3D profile of iridium coated anode (Fig. 4A) shows uniform distribution of iridium and ionomer, which aggregates separately. The surface roughness of iridium coated anode under pressure free condition is extremely high with a thickness error of ±20 μm (Fig. 4B). These two aspects could explain high sensitivity of electrode to mechanical pressure, which is also demonstrated by atomic force microscope (AFM) images with suppressed surface roughness from 157 ± 37 to 76 ± 17 nm under the mechanical pressure from 0 to 5–6 MPa (Figs. S5A and B). Optical microscope and scanning electron microscope (SEM) images show entanglement of Nickel fibers after compression (Fig. 4C–E) and decreased porosity, thus increasing the bulk conductivity of the anode. Mechanical pressure has less effects on the surface conductivity due to non-conductive organic ionomer and the limitation of AFM on porous electrodes (Figs. S5C and D). Meanwhile, mechanical pressure has great impact on contact resistance and hydrophilicity, which can be explained by greatly compressed catalyst-ionomer aggregates, decreased surface roughness that reduce space for wetting but enable better contact (Fig. 4F–K). Consequently, the microstructural evolution of the anode during compression provides reasonable explanations for its changes in physical properties.

**Table 1**
Properties of two anion exchange membranes involved in this study.

| Membrane[a] | Thickness[b] (μm) | Ion Exchange Capacity[c] (meq $OH^-$ $g^{-1}$) | Reinforcement[d] | Conductivity[e] ($mS \cdot cm^{-1}$) |
|---|---|---|---|---|
| AF1-HNN5-25 | 25 | 1.4–1.7 | – | 56 ± 1 |
| AF1-HNN8-50 | 50 | 2.1–2.5 | – | 102 ± 3 |

[a-d] technical specifications (Ionomr Innovation Inc);
[e] From Ref. [23].

After investigating the effects of mechanical pressure on catalyst coated porous electrodes, we then studied their effects on cell activity and stability *etc.* Two typical membranes (Table 1) with the thickness of 25 μm (AF1-HNN5-25) and 50 μm (AF1-HNN8-50) were utilized for ion exchange. It is noteworthy that the AF1-HNN8-50 membrane exhibits

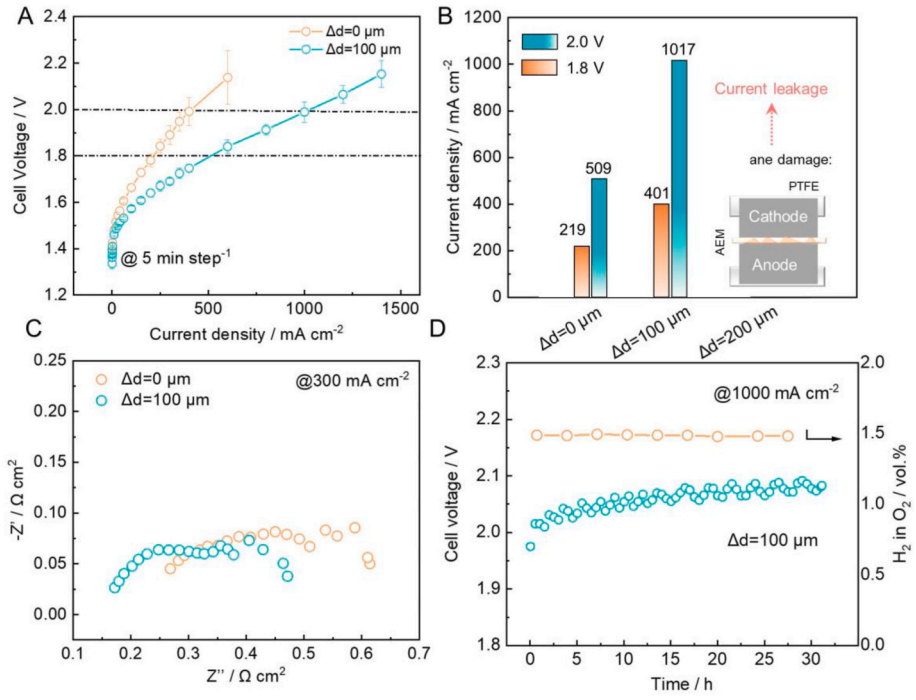


**Fig. 5.** (A) Steady-state polarization curves for the cells employing Pt/C and Ir as cathode and anode catalyst and AF1-HNN5-25 as ion-conducting membrane assembled by different mechanical pressure from 0, 0~0.5 MPa for 5 min step$^{-1}$. (B) Averaged current density at 1.8 and 2.0 V (1–2 MPa causes short-circuit). (C) Electrochemical impedance spectroscopies (EIS) at 300 mA cm$^{-2}$. (D) Short-term stability curve at the current density of 1000 mA cm$^{-2}$ and corresponding hydrogen permeation.

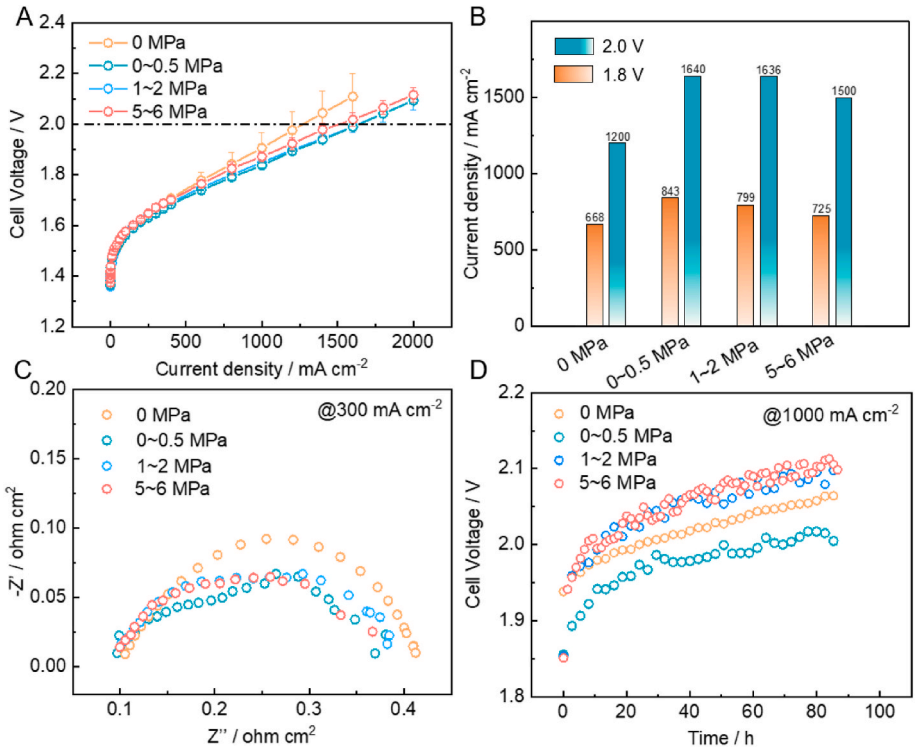


**Fig. 6.** (A) Steady-state polarization curves for the cells employing Pt/C and Ir as cathode and anode catalyst and AF1-HNN8-50 as the io-conducting membrane assembled by different mechanical pressure from 0, 0~0.5, 1–2 to 5–6 MPa for 5 min step$^{-1}$. (B) Averaged current density at 1.8 and 2.0 V. (C) EIS curves at 300 mA cm$^{-2}$ and (D) short-term stability curves at the current density of 1000 mA cm$^{-2}$.

doubled conductivity (102 ± 3 mS cm$^{-1}$) than that of AF1-HNN8-25 (56 ± 1 mS cm$^{-1}$). Due to the fast renewal rate of Aemion + ™ membranes, it is no longer available to obtain membranes with the same chemical composition as the "AF1-HNN8-XX series" in different thicknesses. Therefore, we are compromised to use such membranes, which is not a direct comparison among, but does not affect main conclusions. Iririum

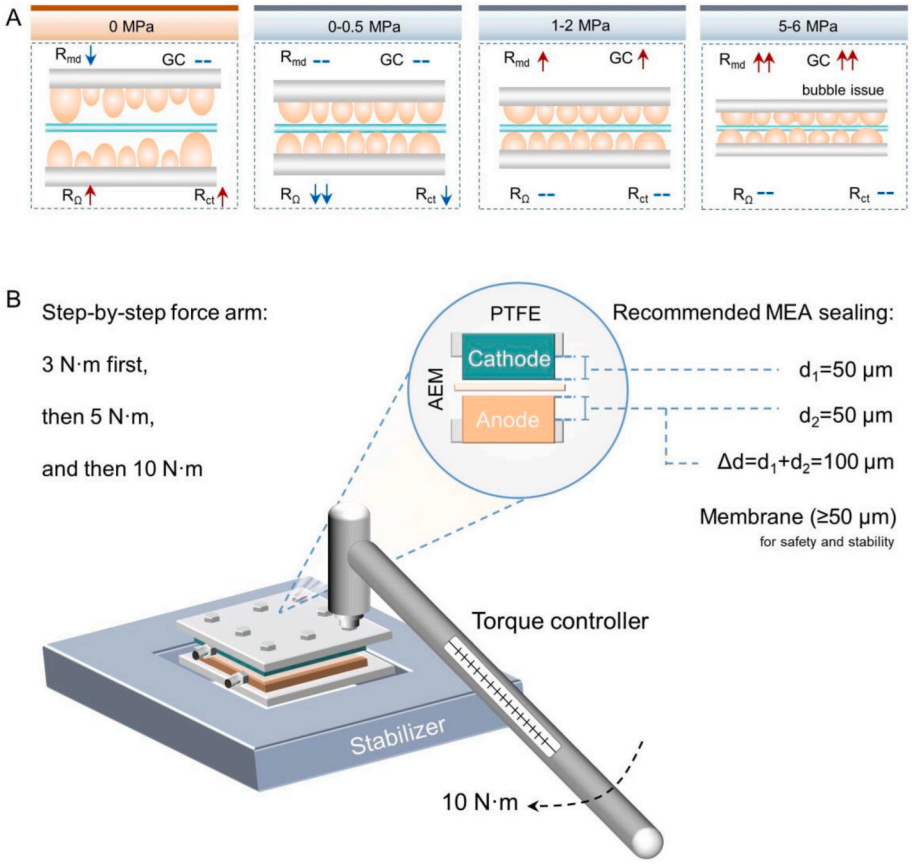


**Fig. 7.** (A) The relationship of ohmic, charge transfer, and mass diffusion resistance (bubble issue) with the mechanical pressure from 0, 0~0.5, 1–2 to 5–6 MPa. (B) Recommended cell assembly steps in such a specific cell structure with eight screws on the outer side general and more generally applicable mechanical pressure of ca. 0.5 MPa for other cell structures.

and platinum represent a commonly studied, commercially available and well-established electrocatalysts in the field, making them a practical starting point for investigating mechanical pressure effects.

The polarization curves for the AF1-HNN5-25 based cells (Fig. 5A and B) show that the current density under 0 MPa is 509 mA $cm^{-2}$ at 2.0 V, while 0~0.5 MPa compressed cells exhibit doubled performance of 1017 mA $cm^{-2}$. EIS plots at three representative current densities of 10, 300 and 1000 mA $cm^{-2}$ (Fig. 5C, Figs. S6A and B) show that the performance enhancement is mainly due to almost halved $R_\Omega$ from ca. 0.22 to 0.145 Ω $cm^2$ and slightly decreased $R_{ct}$ (*e.g.*, from ca. 3.75 to 3.25 Ω $cm^2$ at 10 mA $cm^{-2}$). With the mechanical pressure further increasing to 1–2 MPa, the cell has already failed after only 6 h conditioning at 1.7 V due to membrane damage. This can also be clarified by the abnormal polarization curve beyond theoretical voltage of 1.23 V (Fig. S7A) and 0.001 V open-circuit voltage tested by a multimeter (Fig. S7B). To prevent from safety issue, hydrogen permeation was detected during the short-term stability test (Fig. 5D). The GC of the cell is almost stabilized at ca.1.48%, which is below the standard safety requirement of below 2% [27].

Then the membrane AF1-HNN8-50 with the thickness of 50 μm is further employed to study the effects of higher mechanical pressure from 1–2 to 5–6 MPa) on the cell performance. Similarly, the current density of the cells (Fig. 6A and B) exhibits the same promoting trends by mechanical pressure from 0 to 0~0.5 MPa with the value increasing from 1200 to 1640 mA $cm^{-2}$ at 2.0 V. With further increased mechanical pressure to 1–2 MPa, the current density captured at 2.0 V is more or less stabilized at ca. 1636 mA $cm^{-2}$, attributing to gradually stabilized $R_\Omega$ and $R_{ct}$ (Fig. 6C, Figs. S8A and B). With mechanical pressure increasing to 5–6 MPa, the current density at 2.0 V slightly decreases to 1500 mA $cm^{-2}$. Hydrogen crossover's significance becomes evident, particularly under 5–6 MPa conditions, where the highest hydrogen crossover occurs, reaching levels four times greater than those at 0–0.5 MPa (Fig. S10). Hydrogen crossover may causes faster degradation, which will be discussed later. Our polarization curve data, recorded after a 6-h conditioning period at 1.7 V (supported by Fig. 6D, which indicates a faster initial voltage increase for the 5–6 MPa cell), suggests a potential reduction in current density for cells operating under 5–6 MPa conditions, not merely caused by the electrode invasion (Fig. 2C) but also the blocked electrolyte flow (Fig. S9).

To understand the effect of mechanical pressures on stability, the cells are kept for relative longer time. The cells with the pressure of 0 MPa (Fig. 6D) exhibit a much higher starting voltage of 1.94 V because of the highest $R_\Omega$ and $R_{ct}$, but the lowest voltage fluctuation due to the lowest $R_{md}$. Meanwhile, other cells with the pressure from 0 to 0.5, 1–2 to 5–6 MPa exhibit gradually decreased starting voltage from 1.856, 1.854 to 1.851 V due to suppressed $R_\Omega$ and $R_{ct}$, agreeing well with the bulk and contact resistance (Fig. 3B). However, with the mechanical pressure of 1~2 and 5–6 MPa, the increase of cell voltage is much faster than that with 0 and 0~0.5 MPa, which can be explained by hydrogen crossover associated with accelerated degradation in cell performance in several ways: ***i)*** It diminishes the overall efficiency of the cell since hydrogen oxidation reaction (HOR) occurs, forming HO· and $HO_2$· radicals, subsequently leading to membrane degradation. ***ii)*** These radicals can also poison or deteriorate the electrode materials, causing a decline in the catalytic activity of the catalyst [28]. ***iii)*** Loss of ionomer and membrane degradation can result in pinhole formation and increased gas crossover. As membrane damage and ionomer loss progress, gas crossover intensifies, accelerating the failure of the membrane electrode assembly (MEA) [29].

Consequently, only moderate mechanical pressure ca. 0.5 MPa is

promoting to compressive performance (Fig. 7A), with suppressed $R_\Omega$ and $R_{ct}$ and slightly enhanced $R_{md}$, while excessive mechanical pressure ca. 1–2 and 5–6 MPa greatly increases hydrogen crossover, thus reducing the long-term stability.

After considering the pros ($R_\Omega$/$R_{ct}$) and cons ($R_{md}$, hydrogen crossover, stability, short circuit) of mechanical pressure comprehensively (Fig. 7B), we recommend [30].

i) 0.5 MPa mechanical pressure for cell assembly to suppress $R_\Omega$/$R_{ct}$ and relieve $R_{md}$/hydrogen crossover, which will be greatly affected by both the thickness of gaskets and imposed torque;
ii) Relatively higher membrane thickness (≥50 μm) to prevent from high GC and even short circuit;
iii) Gradually applied mechanical pressure (*e.g.* first 3, then 5, and then 7 N m *etc.*) is preferred for the cell assembly.

## 4. Conclusions

In summary, the mechanical pressure from 0 to 5–6 MPa is of great importance to impact the physical properties of the catalyst coated porous electrodes, especially 68.3% of total bulk and contact resistance on the anode side, 15% reduced electrolyte flow rate, contact angles from 240 ms superwetting to 35000 ms unwetting conditions, *etc.*, and hence further affecting the cell performance. The outstanding contributions of mechanical pressure on the electrode are ***i)*** suppressing contact resistance and ***ii)*** improving the conductivity of bulk electrodes and ***iii)*** slightly enhancing charge transfer processes, while the shortcomings lie in ***i)*** decreased surface hydrophilicity, ***ii)*** blocked mass transfer processes, and ***iii)*** increased gas crossover. Δd and the torque can neither be too large nor too small, only when they are in appropriate ranges (*e.g.* 100 μm and 10 N m in this study) can the best pressure of ca. 0.5 MPa be optimized. To prevent current leakage, the thickness of the membrane is recommended to be ≥ 50 μm. Our study provides a detailed analysis of the effects of mechanical pressure on cell performance, including electron, charge, and mass transfer processes. The reported dominant mechanical pressure of ca. 0.5 MPa best promotes comprehensive cell performance. Moreover, the uncovered non-negligible effects of mechanical pressure may help to better understand one of the most contributing factors and build up inter-lab benchmarks.

## CRediT authorship contribution statement

**Lu Xia:** Conceptualization, Investigation, Visualization, Writing – original draft. **Sebastian Holtwerth:** Investigation. **Christian Rodenbücher:** Investigation. **Werner Lehnert:** Conceptualization, Supervision. **Meital Shviro:** Conceptualization, Supervision. **Martin Müller:** Writing – review & editing.

## Declaration of competing interest

The authors declare that they have no known competing financial interests or personal relationships that could have appeared to influence the work reported in this paper.

## Data availability

Data will be made available on request.

## Acknowledgements

The authors would like to thank Dr. Wulyu Jiang for the help of initiating this study and Shangzhe Yu for some discussion related to electrode deformation.

This work was supported by the Deutsche Forschungsgemeinschaft (DFG, German Research Foundation) – 491111487 and this project has received funding from the European Union's Horizon 2020 research and innovation program under grant agreement No 862509"

## Appendix A. Supplementary data

Supplementary data to this article can be found online at https://doi.org/10.1016/j.jpowsour.2023.233802.

## References

[1] K. Lou, L. Xia, J. Friedrich, M. Shviro, Int. J. Hydrogen Energy (2023), https://doi.org/10.1016/j.ijhydene.2023.08.281.
[2] O. Boström, S. Choi, L. Xia, M. Shviro, F. Lohmann-Richters, P. Jannasch, J. Mater. Chem. A (2023), https://doi.org/10.1039/D3TA03216G.
[3] T. Xiong, B. Huang, J. Wei, X. Yao, R. Xiao, Z. Zhu, F. Yang, Y. Huang, H. Yang, M. Balogun, J. Energy Chem. 67 (2022) 805–813, https://doi.org/10.1016/j.jechem.2021.11.025.
[4] T. Xiong, X. Yao, Z. Zhu, R. Xiao, Y. Hu, Y. Huang, S. Zhang, M. Balogun, Small 18 (2022), 2105331, https://doi.org/10.1002/smll.202105331.
[5] H. Miller, K. Bouzek, J. Hnat, S. Loos, C. Bernäcker, T. Weißgärber, et al., Sustain. Energy Fuels 4 (2020) 2114–2133, https://doi.org/10.1039/C9SE01240K.
[6] I. Vincent, D. Bessarabov, Renew. Sustain. Energy Rev. 81 (2018) 1690–1704, https://doi.org/10.1016/j.rser.2017.05.258.
[7] C. Liu, M. Shviro, A. Gago, S. Zaccarine, G. Bender, P. Gazdzicki, et al., Adv. Energy. Mater. 11 (2021), 2002926, https://doi.org/10.1002/aenm.202002926.
[8] W. Jiang, A. Faid, B. Gomes, I. Galkina, L. Xia, C. Lobo, et al., Adv. Funct. Mater. 32 (2022), 2203520, https://doi.org/10.1002/adfm.202203520.
[9] B. Mayerhöfer, D. McLaughlin, T. Böhm, M. Hegelheimer, D. Seeberger, S. Thiele, ACS Appl. Energy Mater. 3 (2020) 9635–9644, https://doi.org/10.1021/acsaem.0c01127.
[10] C. Liu, K. Wippermann, M. Rasinski, Y. Suo, M. Shviro, M. Carmo, et al., ACS Appl. Mater. Interfaces 13 (2021) 16182–16196, https://doi.org/10.1021/acsami.0c20690.
[11] S. Oener, L. wight, G. Lindquist, S. Boettcher, ACS Energy Lett. 6 (2020) 1–8, https://doi.org/10.1021/acsenergylett.0c02078.
[12] L. Xia, W. Jiang, H. Hartmann, J. Mayer, W. Lehnert, M. Shviro, ACS Appl. Mater. Interfaces 17 (2022) 19397–19408, https://doi.org/10.1021/acsami.2c01302.
[13] D. Xu, M. Stevens, M. Cosby, S. Oener, A. Smith, L. Enman, et al., ACS Catal. 9 (2018) 7–15, https://doi.org/10.1021/acscatal.8b04001.
[14] J. Kaczur, H. Yang, Z. Liu, S. Sajjad, R. Masel, Front. Chem. 6 (2018) 263, https://doi.org/10.3389/fchem.2018.00263.
[15] B. Motealleh, Z. Liu, R. Masel, J. Sculley, Z. Ni, L. Meroueh, Int. J. Hydrogen Energy 46 (2021) 3379–3386, https://doi.org/10.1016/j.ijhydene.2020.10.244.
[16] N. Chen, S. Paek, J. Lee, J. Park, S. Lee, Y. Lee, Energy Environ. Sci. 14 (2021) 6338–6348, https://doi.org/10.1039/D1EE02642A.
[17] A. Niaz, A. Akhtar, J. Park, H. Lim, J. Power Sources 481 (2021), 229093, https://doi.org/10.1016/j.jpowsour.2020.229093.
[18] Q. Xu, S. Oener, G. Lindquist, H. Jiang, C. Li, S. Boettcher, ACS Energy Lett. 6 (2020) 305–312, https://doi.org/10.1021/acsenergylett.0c02338.
[19] I. Vincent, A. Kruger, D. Bessarabov, Int. J. Hydrogen Energy 42 (2017) 10752–10761, https://doi.org/10.1016/j.ijhydene.2017.03.069.
[20] I. Vincent, Int. J. Electrochem. Sci. 13 (2018) 11347–11358, https://doi.org/10.20964/2018.12.84.
[21] N. Lee, D. Duong, D. Kim, Electrochim. Acta 271 (2018) 150–157, https://doi.org/10.1016/j.electacta.2018.03.117.
[22] L. Brown, T. Neville, R. Jervis, T. Mason, P. Shearing, D. Brett, J. Energy Storage 8 (2016) 91–98, https://doi.org/10.1016/j.est.2016.10.003.
[23] P. Fortin, T. Khoza, X. Cao, S. Martinsen, A. Barnett, S. Holdcroft, J. Power Sources 451 (2020), 227814, https://doi.org/10.1016/j.jpowsour.2020.227814.
[24] K. Zhang, R. Zou, Small 17 (2021), e2100129, https://doi.org/10.1002/smll.202100129.
[25] R. Banerjee, N. Bevilacqua, A. Mohseninia, B. Wiedemann, F. Wilhelm, J. Scholta, et al., J. Energy Storage 26 (2019), 100997, https://doi.org/10.1016/j.est.2019.100997.
[26] J. Jin, H. Li, K. Zhao, J. Su, L. Xia, X. Yuan, et al., ACS Appl. Mater. Interfaces 14 (2022) 6157–6166, https://doi.org/10.1021/acsami.1c20726.
[27] M. Kraglund, M. Carmo, G. Schiller, S. Ansar, D. Aili, E. Christensen, et al., Energy Environ. Sci. 12 (2019) 3313–3318, https://doi.org/10.1039/C9EE00832B.
[28] M. Inaba, et al., Electrochim. Acta 51 (2006) 5746–5753, https://doi.org/10.1016/j.electacta.2006.03.008.
[29] S. Vilekar, R. Datta, J. Power Sources 195 (2010) 2241–2247, https://doi.org/10.1016/j.jpowsour.2009.10.023.
[30] L. Xia [D], https://publications.rwth-aachen.de/record/854258/files/854258.pdf, 2022.